Cleaning in place of whey protein fouling - mechanisms of removal

Zhang, Yimin; van den Berg, Frans W.J.; Andersen, Mogens L.; Portela, Luis M.; Parjikolaei, Behnaz Razi; Bakalis, Serafim

DOI
10.1016/j.jfoodeng.2025.112636

Publication date
2025

Document Version
Final published version

Published in
Journal of Food Engineering

Citation (APA)
Zhang, Y., van den Berg, F. W. J., Andersen, M. L., Portela, L. M., Parjikolaei, B. R., & Bakalis, S. (2025). Cleaning in place of whey protein fouling - mechanisms of removal. *Journal of Food Engineering*, *400*, Article 112636. https://doi.org/10.1016/j.jfoodeng.2025.112636

Journal of Food Engineering 400 (2025) 112636

Contents lists available at ScienceDirect

Journal of Food Engineering

journal homepage: www.elsevier.com/locate/jfoodeng

Cleaning in place of whey protein fouling - mechanisms of removal

Yimin Zhang [a], Frans W.J. van den Berg [a], Mogens L. Andersen [a], Luis M. Portela [b], Behnaz Razi Parjikolaei [c], Serafim Bakalis [a,*]

[a] Department of Food Science, University of Copenhagen, Rolighedsvej 26, 1958, Frederiksberg C, Denmark
[b] Transport Phenomena Group, Department of Chemical Engineering, Delft University of Technology, Van der Maasweg 9, 2629HZ, Delft, the Netherlands
[c] Arla Foods Ingredients P/S, Sønderupvej 26, 6920, Videbæk, Denmark

ARTICLE INFO

Keywords:
Cleaning-in-place
Plate heat exchanger
Whey protein fouling
Cleaning models

ABSTRACT

Facing an increased pressure for sustainable manufacturing, the resource demanding but essential process of cleaning-in-place (CIP) requires further optimization. This study aims to understand the mechanisms involved in CIP by designing a process that emulates industrial pasteurization. Whey protein fouling was generated on a stainless-steel metal surface and cleaned the use of an alkaline solution. Cleaning was monitored with optical and UV–Vis spectroscopy measurements recording the fouling thickness and dissolved protein mass in the effluent respectively. Experimental results reveal the mechanisms at play during cleaning, showing a two-stage behavior. The first stage is dominated by the diffusion of NaOH and reaction within the fouling. During the second stage, a drag force peels the fouling from its front edge, assisting removal. The cleaning rate increased with the increase of liquid velocity and temperature. The cleaning rate also depended on the axial location. The cleaning time between two positions 10 cm apart differed by 1.2 min, with a total cleaning time of 5.8 min (at a Reynolds number of 5500 and 70 °C). By developing a model based on observed mechanisms, the study explores using effluent concentration to indicate residual fouling mass and estimate the required cleaning time.

1. Introduction

With an increasing demand for sustainable processing, manufacturers are facing the need to further reduce their environmental impact (Milani et al., 2011). In maintaining sanitation and product stability heat treatment of protein-rich solutions is a fundamental process step in general food manufacturing and specifically for dairies (Burton, 1968; Jimenez et al., 2013). This safety comes at a cost: cleaning-in-place (CIP) accounts for 20 % of the total energy usage, approximately 30 % of the effluent water, and 15–30 % of production downtime in manufacturing (Rad and Lewis, 2014).

For dairy manufacturing pasteurization is an operation commonly used which is especially prone to fouling. It is typically performed in a plate heat exchanger, an operation where the surfaces are particularly susceptible to fouling (Alhuthali et al., 2022; Belmar-Beiny et al., 1993; Petit et al., 2013). During the heating process, proteins denature and deposit on the surfaces of heat exchanger plates. So-called type A fouling deposit is formed under moderate heating around 80 °C. This fouling deposit is yellow, voluminous, and curd-like, and its dry matter consists of about 50 % protein and 35 % 'ash' (Walstra et al., 2005).

To remove fouling material, a typical CIP program for heat exchangers involves several steps: flushing with water to remove any excess materials, treatment with chemicals (base and/or acid) to remove proteins and minerals and, finally, a water flush to remove the CIP chemistry. A base washing step was applied in our study to remove the primary components of the protein fouling layer. It is typically a 0.5 wt% NaOH solution applied at temperatures around 80 °C, with a liquid velocity around 1.5 m s^{-1} (Hagsten et al., 2019; Walstra et al., 2005).

Cleaning of dairy-related fouling layers involves multiple mechanisms (Gillham et al., 1999; Gottschalk et al., 2022). After contact with an alkaline solution, fouling layers first swell (Saikhwan et al., 2010; Wiese et al., 2024). The alkaline diffuses into the fouling layer and reacts. Over time, the alkaline breaks the protein crosslinking inside the fouling layer. Because the cohesion inside is broken, the fouling layer starts to soften (Gillham et al., 1999; Helbig et al., 2022). The protein subsequently disintegrates into the CIP liquid. The weakened cohesion inside the top fouling layer allows removal via an applied shear stress at the interface. While the reaction and removal occur near the interface, the alkaline agent continues to diffuse into and react toward the metal surface. Thus, cleaning the fouling layers from a metal surface is a

* Corresponding author. Rolighedsvej 26 Frederiksberg C, Denmark.
E-mail address: bakalis@food.ku.dk (S. Bakalis).

https://doi.org/10.1016/j.jfoodeng.2025.112636
Received 25 November 2024; Received in revised form 10 April 2025; Accepted 28 April 2025
Available online 29 April 2025

combined effect of mass transfer, chemical reaction, and mechanical abrasion.

Changing conditions affects the processes of diffusion, reaction, and removal. NaOH solution concentration plays a crucial role in determining the chemical reaction rate, with an optimal alkaline concentration identified in prior research (Mercadé-Prieto et al., 2007). At the beginning of the cleaning process, chemical reactions also cause the protein gel to swell (Saikhwan et al., 2010; Pérez-Mohedano et al., 2015). Additionally, temperature has been shown to enhance the rate of the chemical reactions (Fan et al., 2019; Xin et al., 2002) and improve diffusion efficiency (Mercadé-Prieto and Chen, 2006).

The effect of increasing the liquid velocity is more complex (Landel and Wilson, 2021). Since the fouling layer is porous, a higher liquid velocity can also facilitate mass transfer. This occurs either through transporting reacted protein out of the layer or more cleaning chemicals into it. Furthermore, as the chemical reactions weaken the cohesion of the fouling layer (Helbig et al., 2022), a higher liquid velocity can enhance cleaning efficiency through mechanical abrasion.

When working on a (pilot) plant scale, it is important to recognize that the cleaning rate may not be uniform (Xin et al., 2004; Spiegel et al., 2022). Moreover, due to the difficulty in distinguishing the contributions of various mechanisms, predicting the (global) cleaning process becomes challenging. In published studies, the fouling material is not generated directly on the target cleaning metal surface. As a result, the adhesion between the fouling layer and metal surface, which is formed during the heating/pasteurization process, is different (Magens et al., 2019; Zouaghi et al., 2018). Furthermore, during CIP in industry, typical measurements involve analysis on the effluent, while there is a lack of understanding on how they relate to the actual internal surface cleanness.

In this work, we build a transparent channel with a stainless steel bottom to investigate cleaning of dairy fouling deposit. By eliminating complex geometry, this simplified setup allows for a direct understanding of the interaction of fouling deposit with the cleaning solution and surface that is relevant to plate heat exchangers. By flowing a protein solution over a hot metal surface, a fouling layer representative to those observed in larger scales is generated. The subsequent cleaning processes are monitored using image analysis and protein concentration measurements in the effluent. This work aims to quantify cleaning performance at different channel positions. A model is built to use effluent concentration to indicate residual fouling mass and estimate the required cleaning time for each specific run.

2. Experimental setup and materials

2.1. Experimental rig

A rig was designed to simulate a channel in a heat exchanger; a schematic is shown in Fig. 1. Aluminum plate A is the rig's support bottom, stainless steel plate B is the working surface, made from food grade 304 (2B finish) was placed directly on it. Both plates were covered by transparent casing C, forming channel D. The rig was placed on an electric heater (JP Selecta Plactronic) equipped with a temperature controller. The temperature of the metal surface (B) was calibrated against the heater's set temperature by directly measuring on the B surface without liquid. As a result of the efficient heat transferred from A, B could easily reach 80 °C on the working surface. The channel's geometry and size were designed so that the entrance effect will influence only the first 10 cm along the channel, while the exit effect is limited to the last 5 cm (Kundu et al., 2024). The transparent plexiglass C allowed for imaging of the fouling layer during cleaning.

2.2. Deposition of fouling

An experimental procedure was developed to simulate the fouling and cleaning-in-place of an industrial heat exchanger (Fig. 2). Fouling or cleaning liquids were contained in a tank with separate stirring and temperature control (IKA RCT standard). A peristaltic pump (Heidolph PD5001) transferred the liquid into the rig at a calibrated flow rate. The inlet and outlet temperatures were continuously monitored; the channel contents' temperatures was controlled by the bottom heating plate.

Based on the conditions of the pasteurization processes applied in the dairy industry (Walstra et al., 2005) and relevant literature (Petit et al., 2013), a procedure for generating fouling was developed to create reproducible fouling layers. A 10 wt% whey protein concentrated solution (WPC80; AFI LACPRODAN 80; pH at 6.3) was prepared and refrigerated overnight. During the fouling process, 2 L of the WPC solution was maintained at 45 °C in the tank and pumped into the rig at a liquid velocity of 0.28 cm s^{-1} for 1 h, without recirculating. The liquid velocity was deliberately set lower than practical applications to ensure generation of an adequate fouling layer within a reasonable timescale. The temperature of the heating plate was 97 °C, resulting in an outlet temperature of 65 °C. Protein aggregated on the surface of the steel plate (Fig. 1). After each fouling process, plate B was taken out to measure the mass and the thickness of the wet fouling deposit. The thickness at specific streamwise positions (12, 16, 19, and 22 cm downstream) were

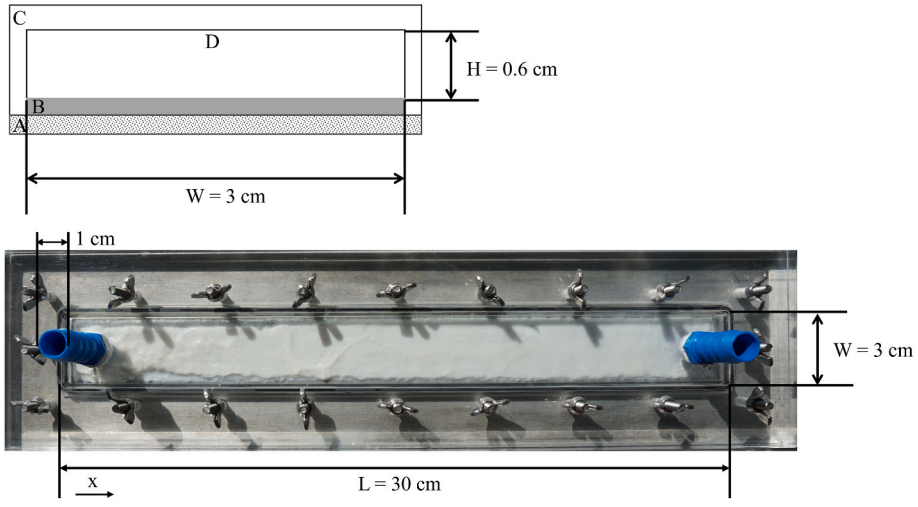

Fig. 1. Schematic cross section (top) and top view (bottom) of the experimental rig, with heated wall A, stainless steel working plate B (width 3 cm, length 30 cm), transparent chamber C and flow channel D (height H = 0.6 cm, width W = 3 cm, length L = 30 cm, volume 54 mL). White layer inside the top view is the fouling deposit.

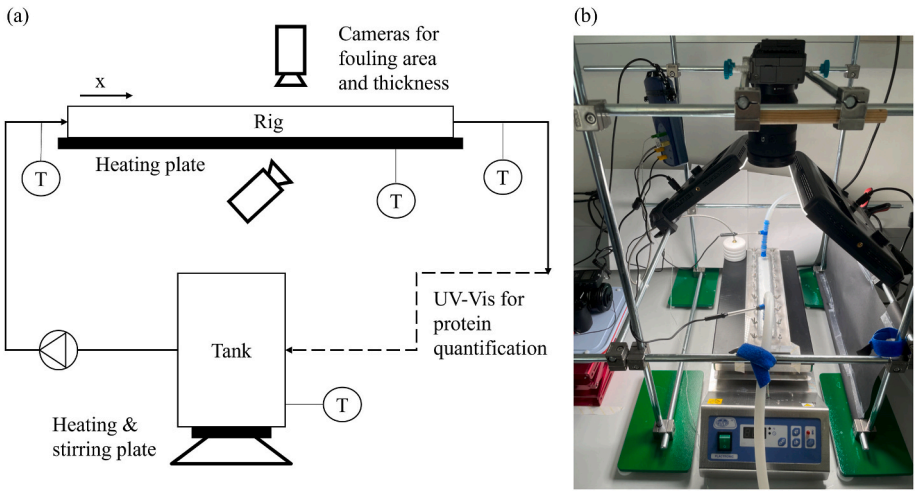

Fig. 2. Experimental setup used for investigating fouling and cleaning of stainless steel surfaces in dairy heat exchangers.

measured using a caliper (accuracy of 0.5 mm). The average fouling thickness was between 2 and 3 mm (Fig. 3). The thickness difference between different positions is less than 0.5 mm within one fouling run. Three separate fouling deposits were generated, their wet mass was measured, and samples were dried overnight at 45 °C to estimate their water content. The moisture content averaged to 86 ± 2.79 wt%, which is close to the value reported in literature (Hooper et al., 2006). Based on data shown in Fig. 3, the fouling layer had a dry matter density at 0.14 ± 0.09 g cm^{-3}. This is a lighter fouling material compared to the wet matter density of 1.05 g cm^{-3} reported in literature (Lalande and Tissier, 1985). This could suggest it is softer than the fouling layer generated with an industrial-level liquid velocity. Morphology of our fouling layer (Fig. A1) resembles that in the literature (Gillham et al., 1999).

2.3. Cleaning of fouling

After height and weight measurements of the fouling, the plate was placed back into the rig for cleaning. For the cleaning-in-place, a 5-L solution of NaOH (0.5 wt% in deionized water) was used as the cleaning agent. CIP conditions typical to those used in the dairy industry were selected (Mercadé-Prieto and Chen, 2006). A pump delivered the cleaning solution at a fixed flow rate ranging from 0.9 to 41.4 mL s^{-1}. The velocities were selected to be relevant to processing, albeit on the lower end of the scale, and allow for use of optical methods for characterisation of the cleaning. At 70 °C, the NaOH solutions were introduced into the rig with mean liquid velocities of 0.5, 1, 1.5, 2, 12, and 23 cm s^{-1}, corresponding to Reynolds numbers of 119, 239, 358, 478, 2868, and 5497 (calculations based on an empty channel). Additional experiments were conducted at 50 °C and 60 °C with a mean liquid velocity of 1 cm s^{-1}. Experiments were conducted both with a closed CIP system, where the cleaning solution was recirculated, and an open CIP system without recirculation, where only fresh cleaning solution passed through the rig. Each cleaning condition was performed at least twice.

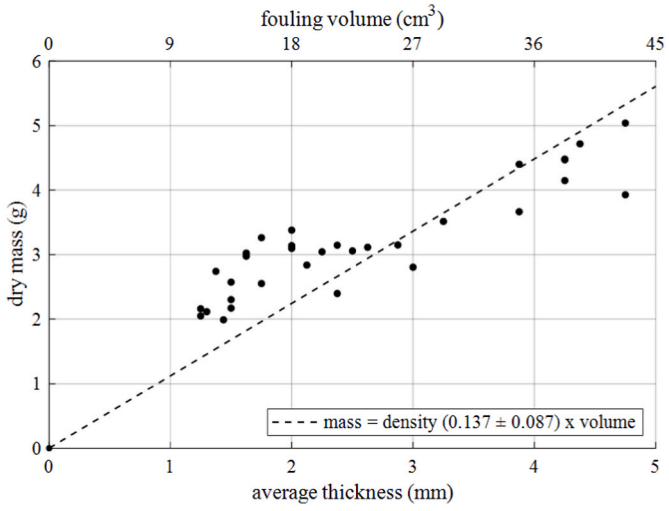

Fig. 3. Dry mass of fouling layers as a function of wet fouling thickness. Data from 32 experiments (including experiments with variable fouling times; R^2 = 0.761). The wet fouling volumes are calculated assuming a total fouling area of 3 × 30 cm^2.

2.4. Image analysis of cleaning

Two methods were used to monitor cleaning progress. Imaging characterized the remaining fouling thickness and UV–Vis spectroscopy (Berg et al., 2017) quantified protein mass inside cleaning solution. One camera was positioned above the rig (Sony FX3, capturing one frame every 5 s at a frame size of 4240 × 600 pixels) to record the fouling-covered area. Another camera was placed on the rig with a side view (Sony Alpha6000, capturing one frame every 5 s at a frame size of 6000 × 300 pixels) to record the thickness of the fouling layer, providing a resolution of 0.03 mm per pixel. The side-view camera was fixed at streamwise position x = 18 cm. The distance between the camera and the rig was set to 46 cm to minimize image deformation.

Fouling layers at different cleaning times and their corresponding thickness were analyzed and quantified by an in-house MATLAB routine (Fig. 4). The fouling layers were identified based on their brightness. Pixels within the top 30 % in terms of brightness were identified as part of the fouling layer. The quantification was not sensitive to the threshold value. For each image (time point) the reported thickness values are averages over 3 mm intervals (1.5 mm upstream and downstream at streamwise positions of 12, 16, 19, and 22 cm).

2.5. Protein in cleaning solution

We conducted experiments with (closed CIP system) and without recirculating (open CIP system). To measure the protein mass dissolved in the cleaning solution, we collected one sample every minute from the tank (closed system) or the effluent flow (open system) in a 3.5 mL cuvette. UV–Vis spectroscopy was used to measure absorbance in the range 260–450 nm (Xin et al., 2004). A set of WPC-NaOH solutions (WPC concentration ranging from 0.1 to 1000 mg L^{-1}; NaOH concentration fixed at 0.5 wt%) was used for calibration based on Multivariate

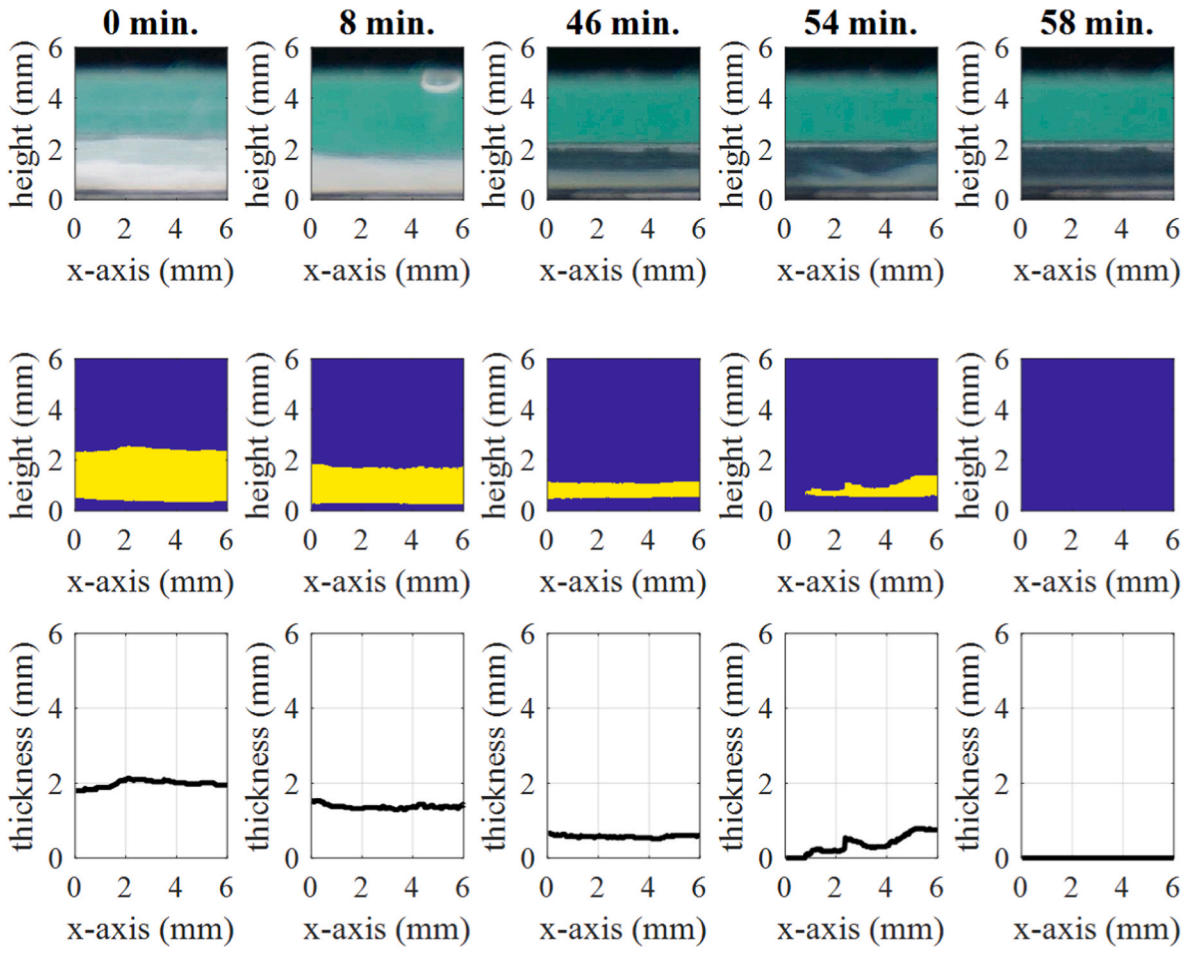

Fig. 4. Side-view images of the fouling layer were used to quantify its thickness at a fixed position during cleaning. Top row: representative image frames at different time points. Middle row: Pixels identified as fouling. Bottom row: Fouling height quantification. $T = 50$ °C, velocity $v = 1.0$ cm s^{-1} (from left to right), position $x = 16$ cm along plate length L. Resolution of 0.03 mm per pixel.

Curve Resolution (Bro and Smilde, 2014; De Juan et al., 2014). The absorbance of the spectrum is directly related to the protein concentration through calibration (Fig. A2); minimum quantifiable concentration was 10 mg L^{-1}. A test run collected samples from different positions in the tank at the same time point during cleaning. UV–Vis absorbance measurements indicated that the concentration differences were below the detection limit of the technique.

3. Results and discussion

Different conditions were used to cleaning the fouling layer. Their effects on the removal rate of fouling (expressed as layer thickness) were quantified. The dependency of the removal rate on streamwise position is emphasized in this section, and a model of cleaning rate is proposed for this dependency. The practical implementation of this model completes our discussion.

3.1. Fouling thickness during cleaning

A typical change of fouling layer (as seen from the side) during cleaning is shown in Fig. 5. The height of the fouling is what we refer to as thickness. Starting from a distinct white appearance (Fig. 5 at 1 min), the fouling changed color and had a relatively slow reduction in thickness with time progressing (Fig. 5, up until ~46 min). The color changed further to brown/yellow, indicating an ongoing chemical reaction. Peeling-off of the fouling layer from the surface happened in the later cleaning stage (Fig. 5, time >46 min). The thickness removal rate increased, which suggests an additional cleaning mechanism.

This acceleration has been observed, but not further discussed in literature (Pérez-Mohedano et al., 2015; Landel and Wilson, 2021; Wiese et al., 2024). The pattern and removal order of the fouling layer suggests the influence of a drag force exerting only at the front edge of the fouling layer (in relation to the flow direction). This force needs to be distinguished from the shear stress, which applies to the entire fouling layer's upper surface. We hypothesize this drag force removal is triggered when NaOH penetrates all the way through the fouling to the metal surface. While the breaking of adhesion to the metal surface allows the fouling to role upwards, the pealed-up fouling's connection to the (downstream) fouling, that is still attached to the metal surface, suggests a retaining of some internal cohesion (Fig. 5).

Fouling thickness curves determined by the analysis of images of different cleaning conditions are shown in Fig. 6. The experiment shown in Fig. 5 corresponds to the same process conditions as in Fig. 6c (black dots). The thickness decline (Fig. 6c) exhibits acceleration around the 45 min mark, which agrees with the phenomena observed in Fig. 5. At the beginning of each CIP cycle, a brief swelling stage exists, shortly before fouling thickness reduction (the first minute, depicted in Fig. A3a). Due to the relatively short duration of this swelling stage compared to the whole cleaning period (Xin et al., 2002), our work (Fig. 6) considers thickness from the time where thickness starts to decline.

The location closer to the fluid entrance takes less time to clean (Fig. 6a). One could assume that the dependence on the axial distance resulted from differences in the initial fouling. To explore this

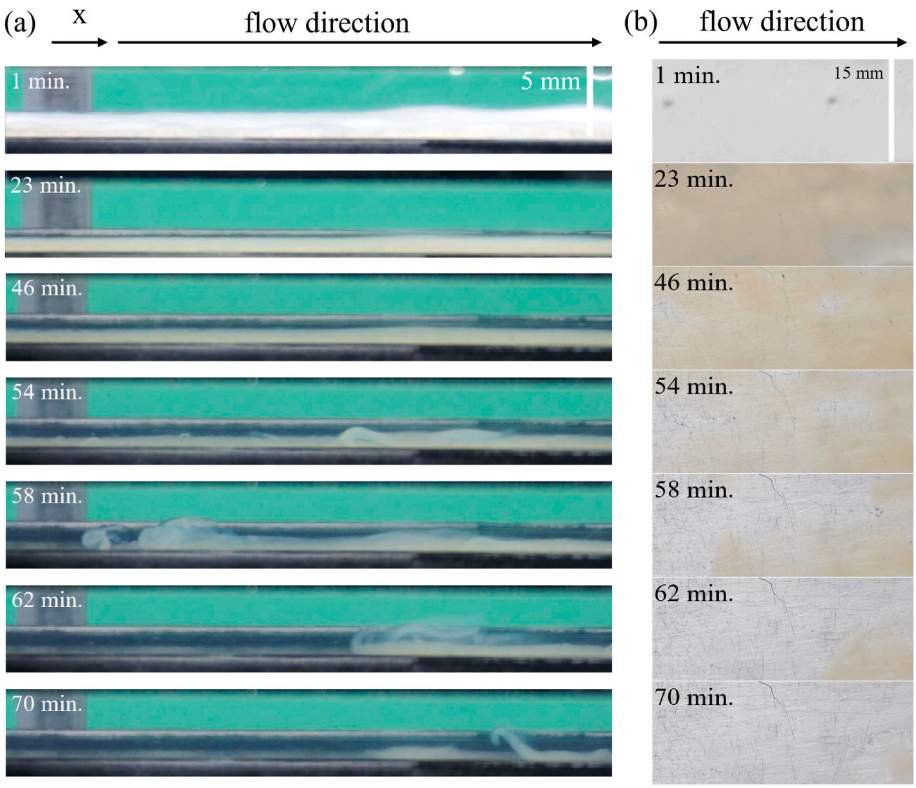

Fig. 5. Frames at different time points during cleaning (temperature $T = 50$ °C, velocity $v = 1.0$ cm s^{-1}, streamwise position $x = 16$–20 cm) of (a) side and (b) top view. In a preliminary experiment without chemicals, physical removal showed the entire fouling layer was white.

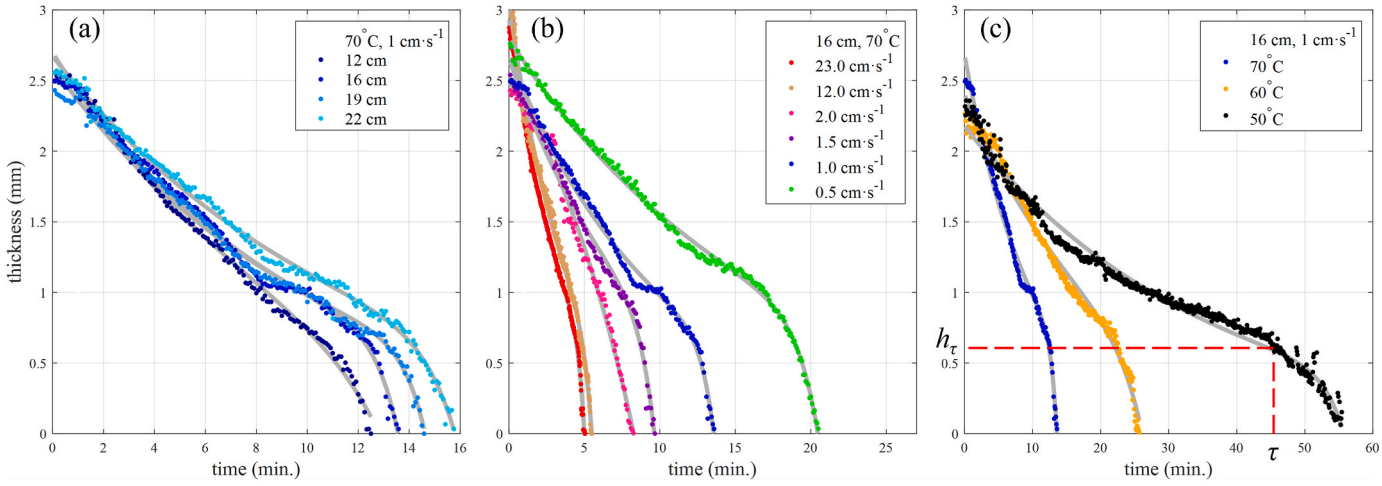

Fig. 6. Selected time-thickness curves (dots) showing the impact of (a) axial distance x (cm), (b) liquid velocity v (cm·s^{-1}), (c) cleaning fluid temperature T (°C). Fitting results with Eq. (1) are shown as grey curves.

hypothesis, we performed a cleaning experiment where we reversed the flow direction, i.e. the cleaning flow entered from what was the fouling flow exit. The kinetics of cleaning were however the same indicating that regardless of the direction of fouling flow, cleaning time increased with streamwise position.

Increasing the liquid velocity accelerates the cleaning, suggesting an influence of shear force (Fig. 6b). However, a 10-min water flush test at 80 °C and 23 cm s^{-1} removed only 0.3 mm of the fouling layer (results not shown). Therefore, softening of the fouling material using chemicals is necessary before mechanical removal. For completeness an experiment conducted with 0.5 wt% NaOH at 70 °C and 23 cm s^{-1} is included in Fig. A3b, showing a similar profile to Fig. 6a. The change in flow regime from laminar (Fig. A3a) to turbulent (Fig. A3b) accelerates the process without changing significantly the trend of removal.

From Fig. 6c one can see that there is a positive effect of temperature on cleaning rate. At 50 °C, the internal cohesion of the fouling allows it to be detached from the metal surface 'in pieces' (Fig. 5). At higher temperatures, we did not observe as clearly this fouling removal by pieces; the boundary between the fouling layer and liquid flow was fuzzier/less distinct at higher temperatures. This is in accordance with published work (Mercadé-Prieto and Chen, 2006; Mercadé-Prieto et al., 2008; Wiese et al., 2024).

To describe the cleaning process, we propose an *ad-hoc* equation to fit fouling thickness curves:

$$h(t) = Ae^{-kt} + Be^{n(t-\tau)} \quad \text{(Eq. 1)}$$

This model uses one exponential for the first stage of the chemical diffusion/reaction stage and one time-delayed exponential for the second stage where an accelerated cleaning was observed. The parameter values were estimated by least square fitting using experimental data; an example fitting is presented in Fig. A4. We found that a straight line could potentially also describe the first stage, particularly for cleaning at higher temperatures (Fig. A3), while at lower temperatures it might not be appropriate. However, using Eq. (1) ensures consistency across different experimental conditions in Fig. 6.

The onset time of peeling-off found by fitting Eq. (1) to the thickness curve in Fig. 6c, agrees with the beginning of peeling off as seen experimentally around 45 min in Fig. 5. The model superimposed in Fig. 6 with grey curves shows a good match with the experiment data. To compare the effect of different cleaning conditions, three key parameters from Eq. (1) were selected: the k of the first cleaning stage which links to the thickness removal rate (dh/dt), transition time point τ, and fouling thickness at this transition time point h_τ.

The decay rate of the first stage k is nearly uniform across different axial distances in Fig. 7a1. A linear increase for transition time τ versus axial distance x can be seen in Fig. 7a2. The drag force applies on the front edge of the fouling layer, and for positions with a longer axial distance, the peeling off thus happened later. When the peeling-off starts, the fouling height was the same, irrespective of the time or axial distance (Fig. 7a3).

The experimental data indicate that, for the first cleaning stage, the thickness decrease rate is nearly independent of the axial distance (Fig. 6a and Fig. A3). From a specific time point onwards, the fouling thickness tends to stay constant and awaits removal in a sequential step. This two-step process can be seen throughout the experiments. A literature source also noted that, although the fouling layer's thickness did not change during their first period, the protein concentration still continuously increased in the solution (Wiese et al., 2024). The authors attributed this constant thickness period to a swelling effect of the fouling layer. We also observed this ongoing fouling mass loss, manifested by the fouling layer gradual transitioning to more transparent, as seen from the top view in Fig. 5.

Increasing liquid velocity removes fouling faster during the first stage (Fig. 6b). This is because a higher shear stress could break stronger cohesion bonds, so the top layer of fouling is removed faster under a higher velocity. The mass transfer of NaOH could simultaneously be facilitated. This also reduces the travel distance of NaOH to the metal surface (Pérez-Mohedano et al., 2015; Landel and Wilson, 2021; Wiese et al., 2024). NaOH arrives at the metal surface within a shorter time, and as a result the peeling off happens earlier with the increasing velocity (Fig. 7b2). A higher liquid velocity also increases the drag force. Experimental results indicated that the increased drag force did not result in peeling of a thicker fouling layer. This suggests that peeling will not occur until NaOH has fully penetrated to the metal surface.

With an increase in liquid velocity, more fouling material is removed during the first stage (Fig. A3). A second cleaning stage occurs irrespective of the conditions in our work. Peeling-off occurs along the

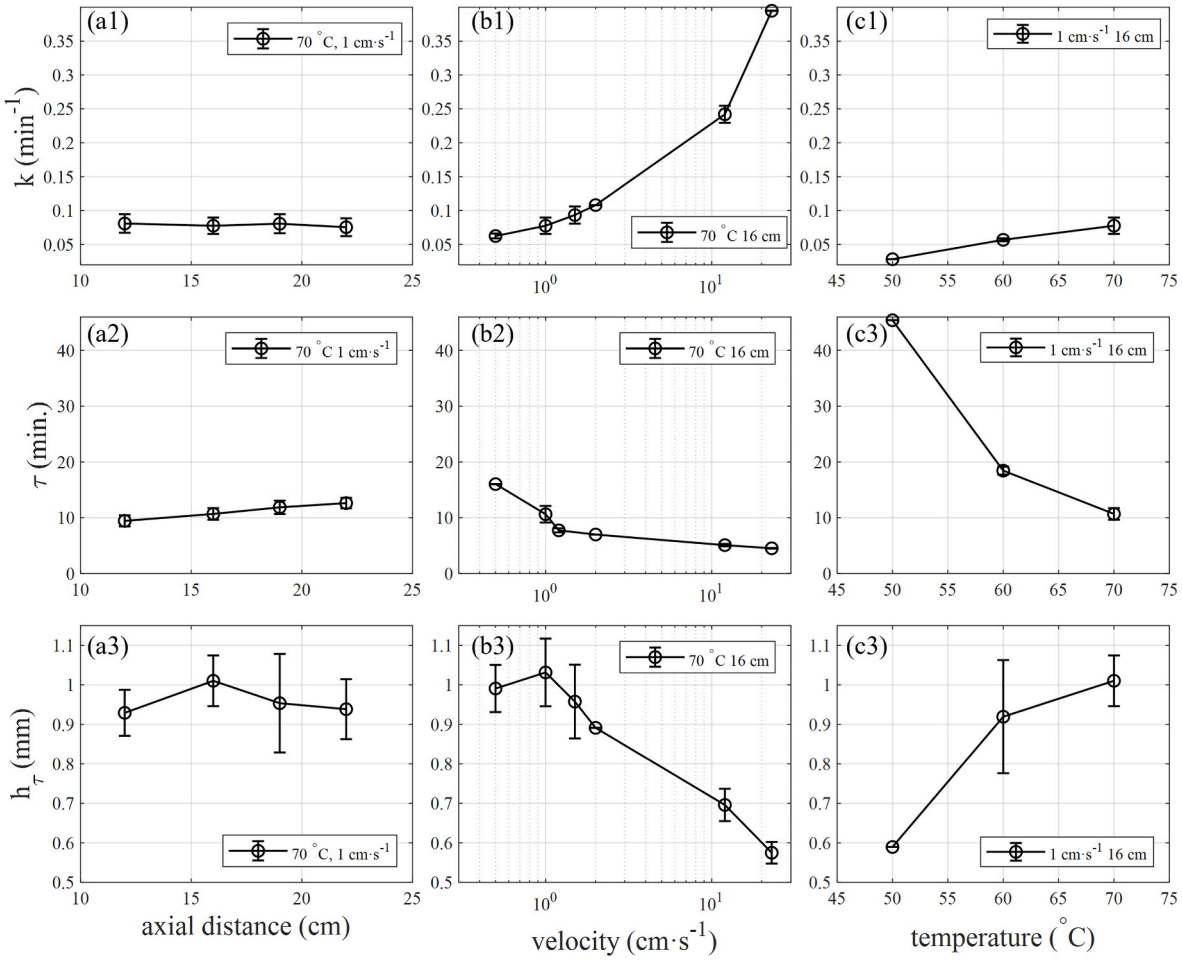

Fig. 7. Effects of cleaning behavior showing (1) decay constant k (min^{-1}), (2) cleaning phase transition time τ (min), (3) fouling height at transition time h_τ (mm) and as a function of (a) streamwise position x (cm), (b) liquid velocity v ($cm{\cdot}s^{-1}$) and (c) cleaning fluid temperature T (°C). Error bars and averages are coming from repeats of experimental conditions.

distance (Figs. 5 and 6). For a cleaning velocity of 1 cm s^{-1}, $x = 12$ cm was clean at 12.2 min, and $x = 22$ cm at 16.8 min. This results in a cleaning time difference of 4.6 min between the two streamwise positions 10 cm apart (Fig. A3a). Using this calculation the moving speed of the fouling material peeled off was estimated at 0.042 ± 0.008 cm s^{-1}. Under a cleaning velocity of 23 cm s^{-1}, the moving speed of the fouling been peeled off was 0.142 ± 0.003 cm s^{-1} (Fig. A3b). The velocity of the fouling front edge is thus much slower than the liquid velocity, consistent with phenomena observed in the literature (Wilson et al., 2014).

The first stage accounts for 79 ± 0.15 % of total cleaning time (Fig. 8a). During this period, an initial fouling layer thickness h_0 of 2.44 ± 0.045 mm is reduced to a transition thickness h_τ of 0.94 ± 0.027 mm (Fig. 8b). The low R^2 value in Fig. 8b indicates that the initial thickness barely influences this transition thickness. Based on the evaluation of each individual curve, the removal rate during the second stage is 2.86 ± 0.81 times faster than that of the first stage.

3.2. Protein concentration curves

Decreasing fouling thickness on the surface leads to an increase in protein concentration in the cleaning solution. In the closed CIP system (i.e., with recirculation, Fig. 9a), as cleaning progresses, protein accumulates and the concentration in the tank increases. The tank concentration is the accumulation of the protein mass removed from the full channel, i.e. along all of the axial distances. When the channel is completely cleaned, no more protein is washed from the metal surface, and the tank concentration will be constant (Wiese et al., 2024).

In the open CIP system (i.e., cleaning solution passing through once, without recirculation, Fig. 9b), the removed protein does not accumulate. It indicates the protein mass removed from all axial positions over a short time period, which can be understood as the cleaning rate at different moments. The cleaning rate increased and then decreased in Fig. 9b. The system needs some minutes to warm up from room temperature to the experiment temperature (Wiese et al., 2024). During this short period the chemical reaction and diffusion is slowly initiated, which is one of the reasons for the increasing cleaning rate at the very beginning. The swelling could also slow down the cleaning at the beginning. With the cleaning progressing, as less fouling is left in the channel, the amount of protein washed away decreases. When the channel is completely cleaned, no more protein is washed from the metal surface, and the removal rate decreases to zero (Gillham et al., 1999; Xin et al., 2002, 2004).

The similar effluent concentration shapes in Fig. 9a indicate a similar cleaning process happening for different velocities. A model describing this cleaning process is built in the next section.

3.3. Effluent concentration based on a local thickness model

In industrial processes, the concentration in the effluent could be measured over time. Therefore, we aimed to better understand the concentration at the effluent. Our approach considers removal across the entire channel as a function of time. The previous model (Eq. (1)) describes the thickness of the fouling layer over time at specific streamwise positions. Building on the understanding of the cleaning process described in section 3.1, this section develops a model to extend the thickness measurements at specific positions to the cleaning rate across different positions over the entire channel. Since mass is conserved, the effluent mass can be predicted using this local thickness model. Comparison with the measured concentration serves to validate the approximation of the observed thickness curve (Fig. 6a). We aim to illustrate that the effluent protein concentration profile during CIP is dominated by the transition from the first stage to the second stage.

Experiments showed two stages during the cleaning process. After a short initial time (heating of the system), the cleaning reaches a constant rate. This rate of removal in the first stage is uniform everywhere in the channel (Fig. 7a1 and Fig. A3). We approximate the exponential used in Eq. (1) by a linear function for simplification (Fig. A3 and Fig. 10a). The second stage cleans faster and relates to τ (Fig. 8a). The transition time point, i.e. switching from the first to the second stage, depends on the streamwise position (Fig. 7a2).

Using the above observations, we construct the model that describes the fouling thickness as a function of time t and streamwise position x in following model steps (Fig. 10b).

1. During the first minute, termed t_{init}, the mass removal rate increases linearly from zero to r_{avg}, the same time for all axial distances (Fig. 9b).
2. This (average) mass removal rate r_{avg} is constant, as can be seen from the straight-line fittings in Fig. 10a.
3. At the transition time point τ, the drag force (stage two mechanism) dominates. As discussed in a previous section (see Fig. 8a) the

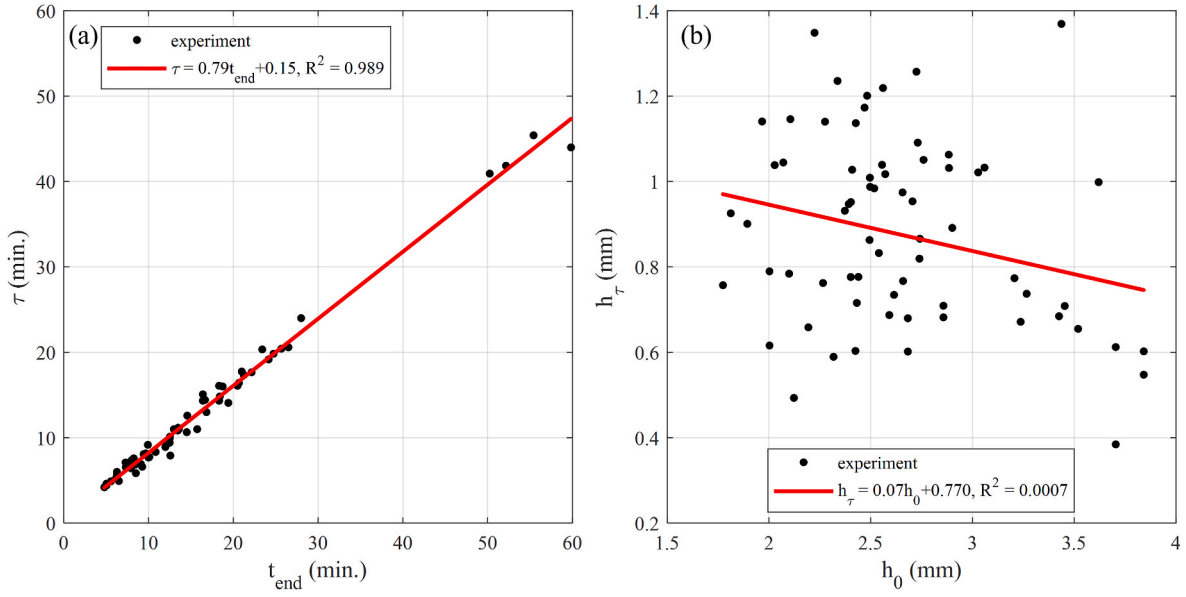

Fig. 8. Linear relationship (based on 32 experiments) between (a) the overall cleaning time t_{end} (min) and the duration of the first stage of cleaning τ (min), (b) initial fouling layer height h_0 (mm) and height at transition time h_τ (mm).

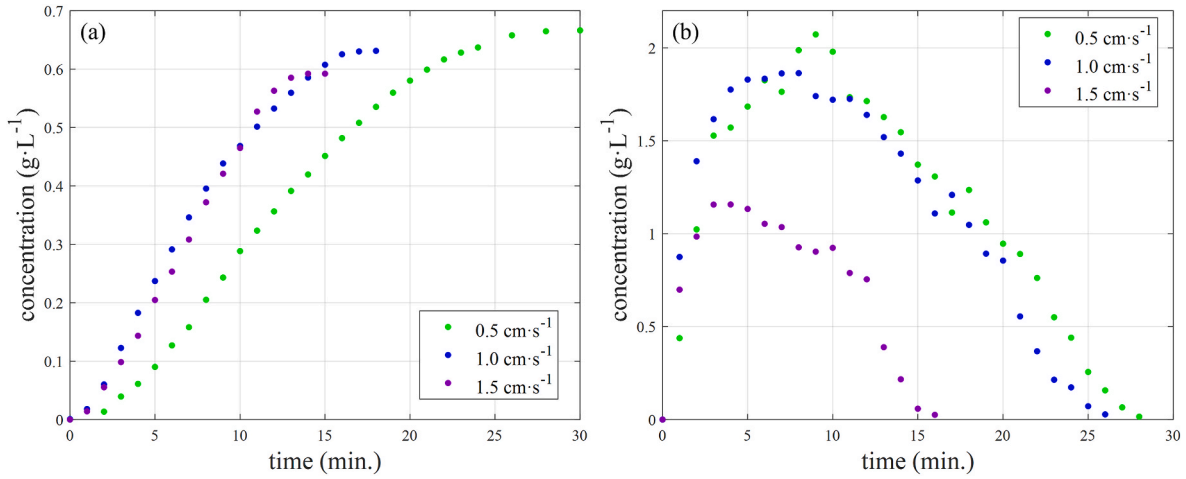

Fig. 9. Time-concentration profiles under different liquid velocities for (a) concentration in the tank C_{tank} (g·L^{-1}) from closed system experiments (CIP with recirculation), (b) effluent concentration C_{out} (g·L^{-1}) from open system experiments (CIP without recirculation); all experiments at 70 °C. Swelling stage is included.

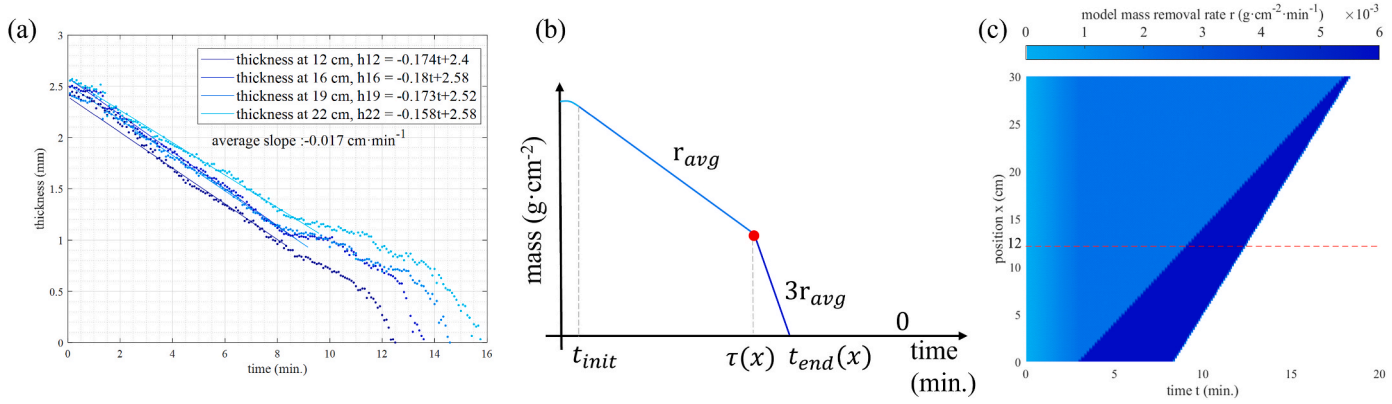

Fig. 10. – Model for mass removal rate derived from (a) thickness curves measured at four positions (70 °C, liquid velocity $v = 1$ cm s^{-1}, position $x = 12$, 16, 19, 22 cm), (b) two stage model of fouling mass removal curve, (c) calculated mass removal rate r (g·cm^{-2}·min^{-1}) time-axial distance contour; the darker the blue, the higher the mass removal rate ($x = 12$ cm marked by dashed line). (For interpretation of the references to color in this figure legend, the reader is referred to the Web version of this article.)

thickness removal rate relates to the rate observed in the first stage and can be approximated by 2.86 r_{avg}.

4. The cleaning rate remains constant until t_{end}, when fouling is fully removed. Beyond t_{end} the mass removal rate drops to 0.

The four steps suggested above are expressed as the global mass removal rate r (g·cm^{-2}·min^{-1}) in Eq. (2):

$$r(x,t) = \begin{cases} \dfrac{t}{t_{init}} r_{avg}, 0 \le t < t_{init} \\ r_{avg}, t_{ini} \le t < \tau(x) \\ 3r_{avg}, \tau(x) \le t < t_{end}(x) \\ 0, t_{end}(x) \le t \end{cases} \quad \text{(Eq. 2)}$$

The axial-averaged mass removal rate r_{avg} is estimated from the thickness removal rate $(dh/dt)_{avg}$ (cm·min^{-1}) in Fig. 10a and the fouling density ρ (g·cm^{-3}):

$$r_{avg} = \rho \frac{dh}{dt}_{avg} \quad \text{(Eq. 3)}$$

A straight line is fitted to the local thickness curves from four selected streamwise positions (12, 16, 19, and 22 cm) to obtain removal rates (dh/dt). The estimated values (Fig. 10a) indicate that these thickness removal rates at different streamwise positions are similar during the first stage. The average of these four local thickness removal rates determines the axial-averaged thickness removal rate, $(dh/dt)_{avg}$. Fouling density is assumed constant, using the dry mass density from Fig. 3 as reference, though it may vary during cleaning.

The onset time point $\tau(x)$ is found from experimental data (Fig. 7a2). A linear relationship between the peeling onset time point $\tau(x)$ (min)

and streamwise position x (cm) is assumed as:

$$\tau(x) = a\,x + b \quad \text{(Eq. 4)}$$

Then transition time points $\tau(x)$ of all streamwise positions can be deducted. The transition time point at the $x = 0$ serves as a reference for the initiation time $t_{init} = \tau(0) = b$. The values of a and b were 0.5 min cm^{-1} and 3 min, respectively (Fig. 10a).

Assuming the initial fouling mass m_0 (g) is evenly distributed across the channel, it results in an initial fouling load σ_0 (g·cm^{-2}), the mass removal rate r across all positions and throughout the cleaning process is shown in Fig. 10c. This model provides an estimation of the protein mass removal by integrating across axial distance and time. With the fixed channel width W (cm), the mass removed $m(x,t)$ (g) from position x to Δx (cm) and from cleaning time t to Δt (min) is:

$$m(x,t) = W \int_{x}^{x+\Delta x} \int_{t}^{t+\Delta t} r(x,t)\, dt\, dx \quad \text{(Eq. 5)}$$

For the closed system, as the cleaning progresses, the concentration in the tank $C_{tank}(t)$ (g·mL^{-1}) equals the washed-out protein (g) over the whole channel length (L = 30 cm) at cleaning time point t (min), dissolved in the total CIP solution volume V (mL), the water content of the fouling layer is assumed negligible compared to the volume of the cleaning solution:

$$C_{tank}(t) = \frac{W \int_0^{30} \int_0^{t} r(x,t)\, dt\, dx}{V} \quad \text{(Eq. 6)}$$

For the open system, the concentration at the outlet $C_{out}(t)$ (g·mL^{-1}) is defined by the mass washed from the entire channel plus the solution volume passing through during the sampling period (min.) as expressed in Eq. (7), where the measurement delay is assumed to be negligible due to the short travel time compared to the total cleaning time:

$$C_{out}(t) = \frac{W \int_0^{30} \int_t^{t+\Delta t} r(x,t)\, dt\, dx}{Q\Delta t} \quad \text{(Eq. 7)}$$

Comparing Eqs. (6) and (7), it can be seen that the tank concentration in the closed system is associated with the total mass of washed-off protein over the entire cleaning duration, while the effluent concentration in the open system is linked to the mass of washed-off protein during a specific time interval of washing. Therefore, by integrating the effluent concentration over time for the open system, we can derive the tank concentration in the closed system.

From the thickness measurements, we can obtain the four parameters of the model (h_0, r_{avg}, a and b using Eqs. (2) and (4)), and then converted these into effluent concentration. Simulated results and experimental data are compared in Fig. 11. The underprediction in Fig. 11b is a result of the (assumed) linear relation between the transition time point $\tau(x)$ and streamwise position x. Incorporating the fitted equation suggested for the thickness measurements (Eq. (1)) instead of our linear approximations did not improve the underprediction. Similar concentration curves have been interpreted from different perspectives (Gillham et al., 1999; Xin et al., 2004; Pérez-Mohedano et al., 2015; Wiese et al., 2024).

3.4. Use of model in an industrial context

Our proposed model is based on local thickness measurements in the lab and is used to estimate the tank concentration and total cleaning time. However, measuring the local fouling thickness is nearly impossible in most real applications. Therefore, to estimate the total cleaning time, we explore the possibility of finding the model parameters from

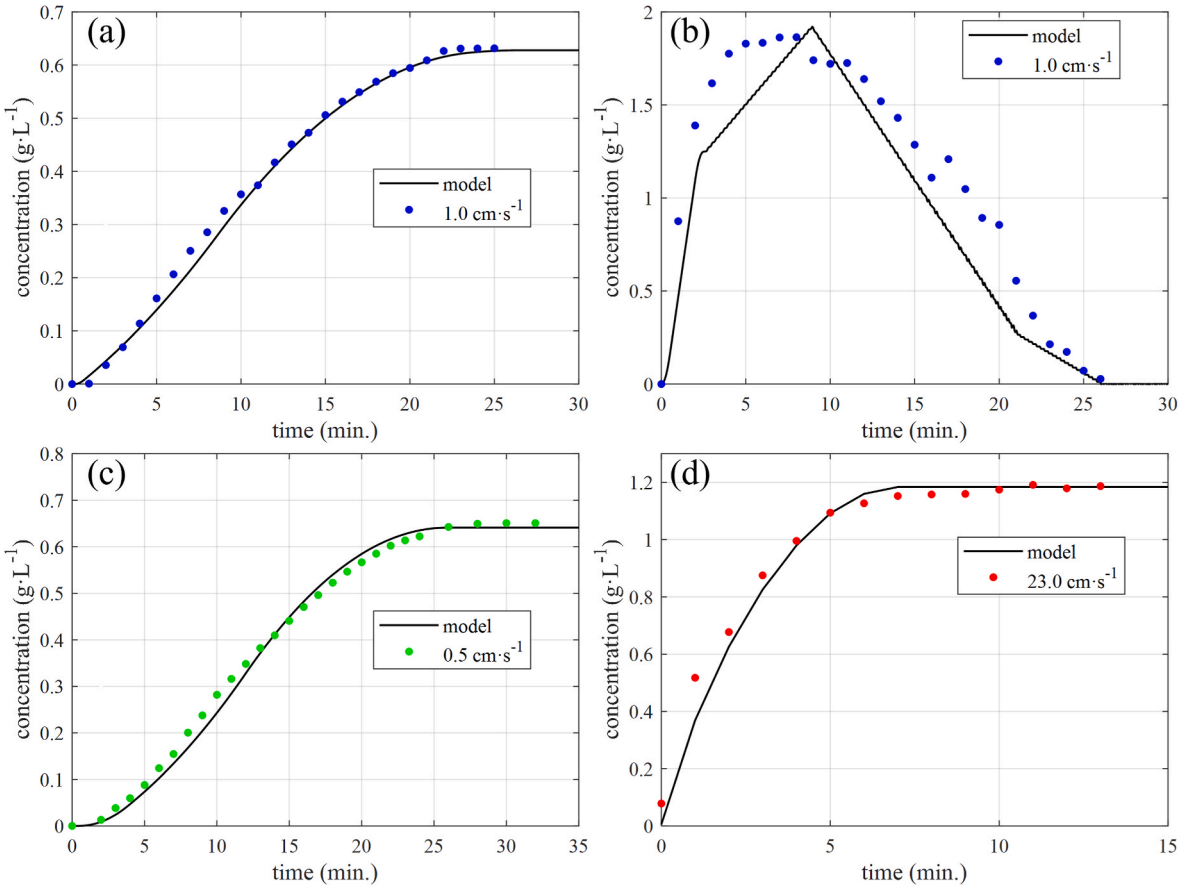

Fig. 11. Cleaning time-concentration profiles for experiment data (dots) and model predictions (lines) for cleaning fluid temperature T = 70 °C under different liquid velocities v (cm·s^{-1}): (a), (c), (d) closed system (CIP with recirculation), (b) open system (CIP without recirculation).

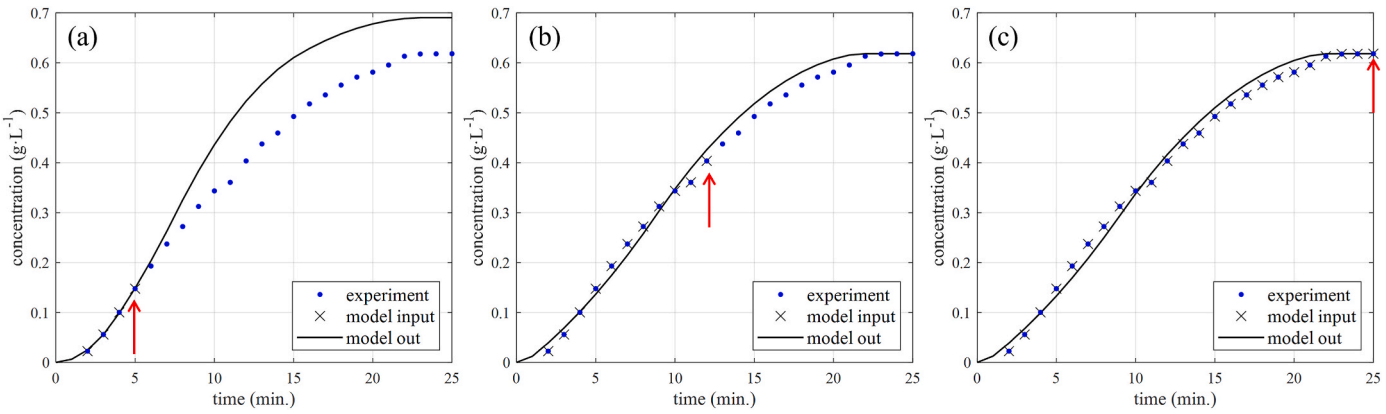

Fig. 12. – Experimental tank concentration profile (dots; temperature $T = 70$ °C, liquid velocity $v = 1$ cm s^{-1}, closed system) and the *real-time* estimated tank concentration of the model based on different amount of data: (a) estimation/extrapolation based on first 5 min, (b) based on 12 min, (c) estimation based on 25 min (total run time). The input data range for the model is marked by a red arrow. (For interpretation of the references to color in this figure legend, the reader is referred to the Web version of this article.)

the protein concentration in the CIP effluent alone.

We tested if our suggested model could estimate the required cleaning time for each specific run based on their online measured concentration. A least squares fitting was used to determine the model parameters (h_0, r_{avg}, a and b; Eqs. (2) and (4)) from measured concentrations. The model was then estimate concentrations in the tank for the following time. Using only the concentration data from the first 5 min as input, the model could already predict that the concentration would stabilize at around 25 min (Fig. 12a). The residual fouling mass corresponding to the open system effluent concentrations could also be estimated (Fig. A5).

Despite a close agreement between experimental data and model estimations, the least squares fitting requires good initial guesses for the parameters. This difficulty arises because the mass removal rate is influenced by both time t and axial distance x, while different combinations of parameters (h_0, r_{avg}, a and b) can lead to the same concentration curve.

Theoretically, the shape of the curves is sensitive to the parameters and can thus be optimized every time a new measurement comes available. The parameter m_0 determines the final tank concentration, r_{avg} influences the rate of the concentration increase, and b dictates the time when the tank concentration begins to rise rapidly (Eqs. (2) and (4)). By focusing on different segments of the concentration curve, we can constrain the values of these parameters, while a better initial guess could be assisted (e.g. constrained optimization) using historical data. To apply this model to the cleaning of a plate heat exchanger, the effect of the wave pattern on its plates (versus our simple flat plate) needs to be investigated. Future applications to large-scale CIP processes in industry are planned to further validate the model.

4. Conclusion

In this work, we developed an experimental setup to generate a reproducible fouling layer. Under different cleaning conditions we measured the reduction of the fouling thickness at different streamwise positions. These thickness curves showed a consistent two-stage profile. In the first stage, the thickness removal rate is influenced by temperature and liquid velocity but shows no correlation with streamwise positions. We attribute this to the dominance of NaOH diffusion into, and reaction with, the fouling layer. In the second stage, the thickness removal rate increases significantly. The fouling layer removal during this stage manifests a streamwise position effect. We attribute this increased rate to activating a flow drag force on the leading edge of the fouling layer.

Based on experimental data, a model for fouling removal rate at different positions and times is derived. This model also estimates the protein concentration washed into the solution, which align well with the measured protein concentrations. Therefore, the effluent concentration reflects the convolution of mass removal rates at different points and times. On the other hand, utilizing effluent concentration to infer fouling thickness requires information on the initial fouling thickness and the onset time of the drag force action. With real-time measurement of concentration, our model achieved sufficient accuracy in predicting the cleaning process of a basic plate heat exchanger system.

Funding

This work was supported by Arla Foods Ingredients, Danish Dairy Research Foundation, and Danish Milk Levy Fund.

CRediT authorship contribution statement

Yimin Zhang: Writing – original draft, Visualization, Validation, Resources, Methodology, Formal analysis, Data curation, Conceptualization. **Frans W.J. van den Berg:** Writing – review & editing, Visualization, Supervision, Methodology, Investigation, Formal analysis, Conceptualization. **Mogens L. Andersen:** Writing – review & editing, Validation, Supervision, Investigation. **Luis M. Portela:** Writing – review & editing, Methodology, Investigation, Funding acquisition. **Behnaz Razi Parjikolaei:** Writing – review & editing, Resources, Investigation, Funding acquisition, Data curation, Conceptualization. **Serafim Bakalis:** Writing – review & editing, Supervision, Project administration, Methodology, Investigation, Funding acquisition, Formal analysis, Conceptualization.

Declaration of competing interest

The authors declare that they have no known competing financial interests or personal relationships that could have appeared to influence the work reported in this paper.

Nomenclature

C (g·L^{-1}) or (g·mL^{-1}) Concentration of protein

C_{out} ($g{\cdot}L^{-1}$) or ($g{\cdot}mL^{-1}$) Concentration at channel outlet
C_{tank} ($g{\cdot}L^{-1}$) or ($g{\cdot}mL^{-1}$) Concentration in the tank
h (mm) Fouling thickness
h_x (mm) Fouling thickness at streamwise position x
h_τ (mm) Fouling thickness at transition-time point
h_0 (mm) Initial fouling thickness
$\frac{dh}{dt}$ ($cm{\cdot}min^{-1}$) or ($mm{\cdot}min^{-1}$) Thickness removal rate
$\frac{dh}{dt}_{avg}$ ($cm{\cdot}min^{-1}$) or ($mm{\cdot}min^{-1}$) Streamwise averaged thickness removal rate
k (min^{-1}) Decay constant of first cleaning stage
L (cm) Length of the channel
m (g) Removed fouling mass
m_0 (g) Initial fouling mass
n (min^{-1}) Decay constant of second cleaning stage
σ_0 ($g{\cdot}cm^{-2}$) Initial fouling mass load
Q ($mL{\cdot}s^{-1}$) or ($mL{\cdot}min^{-1}$) Flow rate
r ($g{\cdot}cm^{-2}{\cdot}min^{-1}$) Mass removal rate
r_{avg} ($g{\cdot}cm^{-2}{\cdot}min^{-1}$) Averaged mass removal rate of the first cleaning stage
t (min) Cleaning time
t_{end} (min) Total cleaning time
t_{init} (min) Initiation time
T (°C) Temperature
τ (min) Transition time point
v ($cm{\cdot}s^{-1}$) Liquid velocity
V (L) or (mL) Tank volume
W (cm) Channel width
x (cm) Streamwise position; axial distance
ρ ($g{\cdot}cm^{-3}$) Fouling dry mass density

Appendix A. Supplementary data

Supplementary data to this article can be found online at https://doi.org/10.1016/j.jfoodeng.2025.112636.

Data availability

Data will be made available on request.

References

Alhuthali, S., Delaplace, G., Macchietto, S., Bouvier, L., 2022. Whey protein fouling prediction in plate heat exchanger by combining dynamic modelling, dimensional analysis, and symbolic regression. Food Bioprod. Process. 134, 163–180. https://doi.org/10.1016/j.fbp.2022.05.009.

Belmar-Beiny, M.T., Gotham, S.M., Paterson, W.R., Fryer, P.J., Pritchard, A.M., 1993. The effect of Reynolds number and fluid temperature in whey protein fouling. J. Food Eng. 19, 119–139. https://doi.org/10.1016/0260-8774(93)90038-L.

Berg, T.H.A., Ottosen, N., Van Den Berg, F., Ipsen, R., 2017. Inline UV-Vis spectroscopy to monitor and optimize cleaning-in-place (CIP) of whey filtration plants. LWT 75, 164–170. https://doi.org/10.1016/j.lwt.2016.08.014.

Bro, R., Smilde, A.K., 2014. Principal component analysis. Anal. Methods 6, 2812–2831. https://doi.org/10.1039/C3AY41907J.

Burton, H., 1968. Section G. Deposits from whole milk in heat treatment plant—a review and discussion. J. Dairy Res. 35, 317–330. https://doi.org/10.1017/S0022029900019038.

De Juan, A., Jaumot, J., Tauler, R., 2014. Multivariate Curve Resolution (MCR). Solving the mixture analysis problem. Anal. Methods 6, 4964–4976. https://doi.org/10.1039/C4AY00571F.

Fan, L., Ge, A., Chen, X.D., Mercadé-Prieto, R., 2019. The role of non-covalent interactions in the alkaline dissolution of heat-set whey protein hydrogels made at gelation pH 2–11. Food Hydrocoll. 89, 100–110. https://doi.org/10.1016/j.foodhyd.2018.10.035.

Gillham, C.R., Fryer, P.J., Hasting, A.P.M., Wilson, D.I., 1999. Cleaning-in-Place of whey protein fouling deposits. Food Bioprod. Process. 77, 127–136. https://doi.org/10.1205/096030899532420.

Gottschalk, N., Augustin, W., Scholl, S., Ian Wilson, D., Mercadé-Prieto, R., 2022. Model food soils for investigating cleaning: a review. Food Bioprod. Process. 136, 249–296. https://doi.org/10.1016/j.fbp.2022.09.013.

Hagsten, C., Innings, F., Trägårdh, C., Hamberg, L., Paulsson, M., Nylander, T., 2019. Removal of UHT dairy fouling — an efficient cleaning process by optimizing the rate controlling alkaline cleaning step. Food Bioprod. Process. 113, 101–107. https://doi.org/10.1016/j.fbp.2018.11.010.

Helbig, M., Majschak, J.-P., Köhler, H., 2022. Direct measurement of the cohesive strength of whey protein gel in contact with NaOH by wire cutting experiments. Food Bioprod. Process. 136, 141–153. https://doi.org/10.1016/j.fbp.2022.09.003.

Hooper, R.J., Paterson, W.R., Wilson, D.I., 2006. Comparison of whey protein model foulants for studying cleaning of milk fouling deposits. Food Bioprod. Process. 84, 329–337. https://doi.org/10.1205/fbp06028.

Jimenez, M., Delaplace, G., Nuns, N., Bellayer, S., Deresmes, D., Ronse, G., Alogaili, G., Collinet-Fressancourt, M., Traisnel, M., 2013. Toward the understanding of the interfacial dairy fouling deposition and growth mechanisms at a stainless steel surface: a multiscale approach. J. Colloid Interface Sci. 404, 192–200. https://doi.org/10.1016/j.jcis.2013.04.021.

Kundu, P.K., Cohen, I.M., Dowling, D.R., Capecelatro, J., 2024. Fluid Mechanics, seventh ed. Academic Press, Amsterdam.

Lalande, M., Tissier, J., 1985. Fouling of heat transfer surfaces related to β-lactoglobulin denaturation during heat processing of milk. Biotechnol. Prog. 1, 131–139. https://doi.org/10.1002/btpr.5420010210.

Landel, J.R., Wilson, D.I., 2021. The fluid mechanics of cleaning and decontamination of surfaces. Annu. Rev. Fluid Mech. 53, 147–171. https://doi.org/10.1146/annurev-fluid-022820-113739.

Magens, O.M., Hofmans, J.F.A., Adriaenssens, Y., Ian Wilson, D., 2019. Comparison of fouling of raw milk and whey protein solution on stainless steel and fluorocarbon coated surfaces: effects on fouling performance, deposit structure and composition. Chem. Eng. Sci. 195, 423–432. https://doi.org/10.1016/j.ces.2018.09.039.

Mercadé-Prieto, R., Paterson, W.R., Wilson, D.I., 2007. The pH threshold in the dissolution of β-lactoglobulin gels and aggregates in alkali. Biomacromolecules 8, 1162–1170. https://doi.org/10.1021/bm0611001.

Mercadé-Prieto, R., Paterson, W.R., Dong Chen, X., Ian Wilson, D., 2008. Diffusion of NaOH into a protein gel. Chem. Eng. Sci. 63, 2763–2772. https://doi.org/10.1016/j.ces.2008.02.029.

Mercadé-Prieto, R., Chen, X.D., 2006. Dissolution of whey protein concentrate gels in alkali. AIChE J. 52, 792–803. https://doi.org/10.1002/aic.10639.

Milani, F.X., Nutter, D., Thoma, G., 2011. Invited review: environmental impacts of dairy processing and products: a review. J. Dairy Sci. 94, 4243–4254. https://doi.org/10.3168/jds.2010-3955.

Pérez-Mohedano, R., Letzelter, N., Bakalis, S., 2015. Development of a swelling-removal model for the scanning fluid dynamic gauge. Food Bioprod. Process. 93, 269–282. https://doi.org/10.1016/j.fbp.2014.10.001.

Petit, J., Six, T., Moreau, A., Ronse, G., Delaplace, G., 2013. β-lactoglobulin denaturation, aggregation, and fouling in a plate heat exchanger: pilot-scale experiments and dimensional analysis. Chem. Eng. Sci. 101, 432–450. https://doi.org/10.1016/j.ces.2013.06.045.

Rad, S.J., Lewis, M.J., 2014. Water utilisation, energy utilisation and waste water management in the dairy industry: a review. Int. J. Dairy Technol. 67, 1–20. https://doi.org/10.1111/1471-0307.12096.

Saikhwan, P., Mercadé-Prieto, R., Chew, Y.M.J., Gunasekaran, S., Paterson, W.R., Wilson, D.I., 2010. Swelling and dissolution in cleaning of whey protein gels. Food Bioprod. Process. 88, 375–383. https://doi.org/10.1016/j.fbp.2010.09.006.

Spiegel, C., Aselmeyer, F., Augustin, W., Scholl, S., 2022. Quantification method for cleaning-in-place procedures in micro structured equipment. Food Bioprod. Process. 134, 150–162. https://doi.org/10.1016/j.fbp.2022.05.010.

Walstra, P., Walstra, Pieter, Wouters, J.T.M., Geurts, T.J., 2005. Dairy Science and Technology, second ed. CRC Press.

Wiese, H., Geißler, H., Augustin, W., Scholl, S., 2024. Diffusive mass transfer and protein removal in the alkaline cleaning of a jellylike whey protein fouling layer. Heat Mass Tran. 60, 829–840. https://doi.org/10.1007/s00231-023-03391-7.

Wilson, D.I., Atkinson, P., Köhler, H., Mauermann, M., Stoye, H., Suddaby, K., Wang, T., Davidson, J.F., Majschak, J.-P., 2014. Cleaning of soft-solid soil layers on vertical and horizontal surfaces by stationary coherent impinging liquid jets. Chem. Eng. Sci. 109, 183–196. https://doi.org/10.1016/j.ces.2014.01.034.

Xin, H., Chen, X.D., Özkan, N., 2002. Whey protein-based gel as a model material for studying initial cleaning mechanisms of milk fouling. J. Food Sci. 67, 2702–2711. https://doi.org/10.1111/j.1365-2621.2002.tb08802.x.

Xin, H., Chen, X.D., Özkan, N., 2004. Removal of a model protein foulant from metal surfaces. AIChE J. 50, 1961–1973. https://doi.org/10.1002/aic.10149.

Zouaghi, S., Six, T., Nuns, N., Simon, P., Bellayer, S., Moradi, S., Hatzikiriakos, S.G., André, C., Delaplace, G., Jimenez, M., 2018. Influence of stainless steel surface properties on whey protein fouling under industrial processing conditions. J. Food Eng. 228, 38–49. https://doi.org/10.1016/j.jfoodeng.2018.02.009.